10198 *Biochemistry* **2010,** *49,* 10198–10207
DOI: 10.1021/bi101303t

BIOCHEMISTRY
including biophysical chemistry & molecular biology
Article

Structural Basis of Ubiquitin Recognition by Translesion Synthesis DNA Polymerase ι[†]

Gaofeng Cui,[‡] Robert C. Benirschke,[‡] Han-Fang Tuan, Nenad Juranić, Slobodan Macura, Maria Victoria Botuyan, and Georges Mer*

Department of Biochemistry and Molecular Biology, Mayo Clinic College of Medicine, Rochester, Minnesota 55905, United States.
[‡]G.C. and R.C.B. contributed equally to this work.

Received August 13, 2010; Revised Manuscript Received October 10, 2010

ABSTRACT: Cells have evolved mutagenic bypass mechanisms that prevent stalling of the replication machinery at DNA lesions. This process, translesion DNA synthesis (TLS), involves switching from high-fidelity DNA polymerases to specialized DNA polymerases that replicate through a variety of DNA lesions. In eukaryotes, polymerase switching during TLS is regulated by the DNA damage-triggered monoubiquitylation of PCNA. How the switch operates is unknown, but all TLS polymerases of the so-called Y-family possess PCNA and ubiquitin-binding domains that are important for their function. To gain insight into the structural mechanisms underlying the regulation of TLS by ubiquitylation, we have probed the interaction of ubiquitin with a conserved ubiquitin-binding motif (UBM2) of Y-family polymerase Polι. Using NMR spectroscopy, we have determined the structure of a complex of human Polι UBM2 and ubiquitin, revealing a novel ubiquitin recognition fold consisting of two α-helices separated by a central *trans*-proline residue conserved in all UBMs. We show that, different from the majority of ubiquitin complexes characterized to date, ubiquitin residue Ile44 only plays a modest role in the association of ubiquitin with Polι UBM2. Instead, binding of UBM2 is centered on the recognition of Leu8 in ubiquitin, which is essential for the interaction.

The cellular response to DNA damage comprises DNA repair pathways, which maintain the integrity of the genetic material, as well as DNA damage tolerance mechanisms that can lead to mutagenesis (*1*). Translesion DNA synthesis (TLS)[1] is a DNA damage tolerance process that rescues the stalled replication machinery through its ability to bypass bulky DNA lesions (*2*, *3*). This process is carried out by specialized DNA polymerases known as mutagenic or error-prone polymerases and is conserved in all three kingdoms of life. In contrast to high-fidelity polymerases that stall at DNA lesions, TLS polymerases, the majority of which belong to the so-called Y-family (*4*), are capable of adding nucleotides to the replicating strand opposite the lesion, albeit with low fidelity (*5*−*7*).

How DNA replication can switch to TLS at sites of DNA damage is unclear, but essential to this process in eukaryotes is the damage-triggered monoubiquitylation at Lys164 of proliferating cell nuclear antigen (PCNA) (*8*), a DNA sliding clamp required for optimal DNA polymerase processivity or efficiency of nucleotide incorporation. The first identified Y-family member, Rev1 (*9*), is thought to be constitutively bound to PCNA through an N-terminal BRCT domain (*10*, *11*) and to be activated upon monoubiquitylation of PCNA (*12*−*14*). Rev1 preferentially incorporates dCMP opposite dGMP or apurinic/apyrimidinic sites in DNA (*15*, *16*). Rev1 also plays a key adaptor role in TLS by facilitating the recruitment of specialized polymerases, including all Y-family members, to DNA damage sites, thereby allowing bypass of a variety of DNA lesions (*17*).

Progress has been made toward understanding the molecular mechanisms by which Rev1 and monoubiquitylated PCNA ($PCNA^{Ub}$) control the switching from high-fidelity polymerases to TLS polymerases and switching among TLS polymerases (*18*). It was found that a conserved motif at the C-terminus of Rev1 determines its association with all other Y-family polymerases, namely, Polη, Polκ, and Polι in higher eukaryotes (*19*−*22*). Polη, Polκ, and Polι can also bind PCNA by means of a consensus PCNA-interaction peptide (PIP) sequence located in their C-terminal region (*23*−*27*). Moreover, these three polymerases as well as Rev1 present ubiquitin-binding domains at their C-terminus, which are required for TLS and interaction with $PCNA^{Ub}$ (*28*, *29*). There is one ubiquitin-binding zinc finger (UBZ) domain in Polη and two in Polκ, while Polι and Rev1 each possess two ubiquitin-binding motifs (UBM1 and UBM2) important for their role in the tolerance of DNA damage (*28*, *30*, *31*).

To further our understanding of the switch mechanisms that trigger TLS, a detailed biophysical characterization of the multiple interaction interfaces involved in the regulated association of TLS polymerases with Rev1 and $PCNA^{Ub}$ is needed. To start filling these gaps in knowledge, we have probed the interactions of Polι UBMs with ubiquitin. We have determined the three-dimensional (3D) structure of human Polι UBM2 in the free state and in complex with ubiquitin, revealing a novel ubiquitin recognition fold consisting of two contiguous α-helices at a sharp angle relative to one another, separated by a conserved *trans*-proline residue. We show that this new motif recognizes Leu8 of ubiquitin, which is essential for the interaction. Through mutagenesis and 3D structure determination we show that this new ubiquitin recognition fold and binding mode are determined by a hydrophobic core in UBM2.

[†]This research was supported in part by National Institutes of Health Grants CA109449 and CA132878 to G.M.

*Corresponding author. Telephone: 507-266-0451. Fax: 507-284-1209. E-mail: mer.georges@mayo.edu.

[1]Abbreviations: BRCT, breast cancer carboxy-terminal; HSQC, heteronuclear single-quantum coherence; NOE, nuclear Overhauser enhancement; NOESY, NOE spectroscopy; TLS, translesion DNA synthesis; UBD, ubiquitin-binding domain; UBM, ubiquitin-binding motif.

 Published on Web 11/04/2010

MATERIALS AND METHODS

Protein Preparation. Human polymerase ι (Polι) DNA corresponding to UBM2 (residues 679−707 and residues 674−715) was cloned into the pTEV expression vector derived from pET15b (Novagen) encoding a tobacco etch virus (TEV) protease-cleavable N-terminal $(His)_6$ tag. Proteins were produced in *Escherichia coli* BL21 (DE3) cells grown in Luria−Bertani broth or M9 minimum media containing 1 g/L $[^{15}N]NH_4Cl$, 4 g/L unlabeled glucose or 2 g/L ^{13}C-enriched glucose, and 1 g/L Isogro or 10% (v/v) Silantes OD2 media that are ^{15}N- or $^{15}N/^{13}C$-enriched (*32*). Stable isotope-enriched reagents were purchased from Isotec and CIL. Cells were grown at 37 °C to an OD_{600} of ∼0.8, transferred to 15 °C, induced with 1 mM final concentration of isopropyl β-D-1-thiogalactopyranoside after 45 min, and then grown for another 16−20 h before harvesting by centrifugation. Cell pellets were resuspended in 50 mM sodium phosphate, pH 7.5, and 300 mM NaCl (solution 1) with 5 mM imidazole and ∼10 mM phenylmethanesulfonyl fluoride and then ruptured using an Emulsiflex C-5 high-pressure homogenizer (Avestin, Inc.). The soluble and insoluble fractions were separated by centrifugation, and the lysate was loaded onto a Ni^{2+}-NTA column (Qiagen). The loaded column was washed with solution 1 with 20 mM imidazole, and the protein was eluted with solution 1 with 500 mM imidazole. The $(His)_6$ tag was removed by incubation with TEV protease overnight at room temperature, leaving the GHM sequence at the N-terminus. Further purification was done with size exclusion chromatography using a Superdex 75 column (GE Healthcare) and by reversed-phase chromatography using a C18 preparative column (Phenomenex).

For NMR structure determination of Polι UBM2−ubiquitin and Polι UBM2 P692A−ubiquitin complexes, samples of unlabeled, ^{15}N-labeled, and $^{15}N/^{13}C$-labeled human ubiquitin (residues 1−76) were prepared with no tag in *E. coli* BL21 (DE3) cells using the plasmid pRSUb (*33*). Cells were grown and ruptured as reported above after which ubiquitin in the cell lysate was purified by a combination of ammonium sulfate precipitation, anion-exchange chromatography, and gel filtration chromatography as previously published (*34*). For ITC measurements and NMR titrations, ubiquitin was cloned in a pT7.7 expression plasmid encoding a noncleavable N-terminal $(His)_6$ tag. Expression and purification of nonlabeled ubiquitin were done as reported above for the UBM2 domain but omitting the $(His)_6$ tag cleavage step.

All mutations in Polι and ubiquitin were introduced using the QuikChange protocol (Stratagene), and mutant proteins were purified as described above. Protein concentrations were determined by UV spectrophotometry using molar extinction coefficients calculated from the amino acid composition.

NMR Spectroscopy. All NMR experiments were performed at 25 °C with a Bruker Avance III 700 MHz spectrometer equipped with a ^1H, ^{15}N, ^{13}C CryoProbe. The protein samples were prepared in 20 mM sodium phosphate, pH 7.0, 30 mM NaCl, and 90% H_2O/10% D_2O.

For resonance assignment and structure determination of the protein complexes, two different samples were prepared, each made up of a labeled and a nonlabeled component. For the Polι UBM2−ubiquitin structure, the concentrations were 0.5 mM $^{15}N/^{13}C$-labeled UBM2 and 2.5 mM unlabeled ubiquitin (sample 1) and 1 mM $^{15}N/^{13}C$-labeled ubiquitin and 3.5 mM unlabeled UBM2 (sample 2). For the Polι UBM2 P692A−ubiquitin structure, the concentrations were 1 mM $^{15}N/^{13}C$-labeled UBM2 P692A and 3 mM unlabeled ubiquitin (sample 1) and 1.5 mM $^{15}N/^{13}C$-labeled ubiquitin and 5 mM unlabeled UBM2 P692A (sample 2). For structure determination of Polι UBM2 in the free state, the $^{15}N/^{13}C$-labeled protein was at a concentration of 1 mM.

The ^1H, ^{15}N, and ^{13}C resonances for each structure were assigned by recording standard triple-resonance NMR spectra (*35*, *36*). 2D $^1H-^{15}N$ HSQC, $^1H-^{13}C$ HSQC, 3D HNCACB, 3D CBCA(CO)NH, 3D HNCO, 3D HN(CA)CO, 3D (H)CC(CO)-NH-TOCSY, 3D H(CC)(CO)NH-TOCSY, 3D $^1H-^{15}N$ TOCSY-HSQC, 3D HBHA(CO)NH, and 3D (H)CCH-TOCSY were used for backbone and side chain resonance assignments. Resonances of aromatic groups were assigned using 2D $^1H-^{13}C$ HSQC and 3D aromatic ^{13}C-edited NOESY-HSQC spectra. Distance restraints for structure determination were generated from 3D ^{15}N- and ^{13}C-edited NOESY spectra (aliphatic and aromatic) as well as 3D ^{13}C, ^{15}N-filtered, ^{13}C-edited NOESY spectra (*37*). All NOESY experiments had a mixing time of 120 ms. NMR spectra were processed using NMRPipe (version 2.1) (*38*) and analyzed using NMRView (version 5.0.4) (*39*).

Structure Calculations. All interproton distances derived from the different NOESY spectra were included in the structure calculations, but note that the numbers of restraints given in Table 1 correspond to nonredundant distances only. The distance restraints were classified into five categories corresponding to upper distance limits of 2.8, 3.5, 4.5, 5.5, and 7 Å. Distance restraints corresponding to hydrogen bonds identified from $^1H/^2H$ exchange experiments were also included. The upper limits for the distances between N and O and between HN and O were set to 3.2 and 2.2 Å, respectively. All distance restraints were set with a lower limit of 1.8 Å. Dihedral angle restraints ϕ and ψ were derived from TALOS (*40*) and CSI (*41*) analysis and included in the calculations with a tolerance of ±30°.

The structures of ubiquitin and UBM2 were first calculated independently with the simulated annealing protocol of CYANA (version 2.1) (*42*) using the intramolecular distance and angle restraints for each protein. Then, these restraints were combined with intermolecular distances to calculate the structures of the complexes. Several iterations of CYANA and SANE (*43*) calculations were performed to help assign nuclear Overhauser enhancement signals (NOEs) and derive distance restraints. Finally, 200 structures of the complexes were calculated of which 100 structures with the lowest energy were refined with AMBER 8 (*44*). The structures were subjected to 20 ps, 20000 steps, of simulated annealing using a generalized Born solvent model (*45*). The system was heated to 1000 K during the first 5 ps, maintained at 1000 K for 3 ps, annealed for 11 ps, and gradually cooled to 0 K over the last 1 ps. The force constants were 20 kcal mol^{-1} $Å^2$ for distance restraints, 50 kcal mol^{-1} rad^{-2} for dihedral angle restraints, 100 kcal mol^{-1} rad^{-2} for chirality restraints, and 150 kcal mol^{-1} rad^{-2} for omega angle restraints. The 20 structures with the lowest AMBER energy were retained for final analysis. The structural statistics are given in Table 1. The quality of final structures was assessed by PROCHECK-NMR (*46*). PyMol (http://www.pymol.org/) was used to create all molecular representations.

Isothermal Titration Calorimetry (*ITC*). ITC measurements were carried out at 10 °C using a VP-ITC titration calorimeter (GE Healthcare). Polι UBM2 and ubiquitin samples were prepared in 50 mM Tris-HCl, pH 7.2, and 30 mM NaCl. Wild-type or mutated UBM2 placed in the calorimeter injection syringe at concentrations ranging from 1 to 2.8 mM was delivered to the reaction cell containing wild-type or mutated ubiquitin at a concentration of 100 μM. A complementary experiment was done in which wild-type ubiquitin was placed in the injection

Table 1: NMR Restraints and Structural Statistics

	ubiquitin−Polι UBM2	Polι UBM2	ubiquitin−Polι UBM2 P692A mutant
no. of NMR restraints			
total NOE restraints	2758	367	3095
intraresidue (*i*, *i*)	635	134	728
sequential ($\|i - j\| = 1$)	662	91	703
medium range ($2 \leq \|i - j\| \leq 4$)	554	105	636
long range ($\|i - j\| > 4$)	768	37	857
intermolecular NOEs	139	N/A	171
hydrogen bond restraints	51	11	53
dihedral angle restraints			
ϕ	73	21	73
ψ	75	24	74
violation analysis			
maximum distance violation (Å)	0.30	0.22	0.28
maximum dihedral angle violation (deg)	0	0	0
energies			
mean AMBER energy (kcal mol^{-1})	−6003.55	−1470.59	−6694.78
mean restraint energy (kcal mol^{-1})	83.31	8.82	82.69
rmsd from idealized geometry			
bond lengths (Å)	0.0083 ± 0.0001	0.0076 ± 0.0001	0.0084 ± 0.0001
bond angles (deg)	2.20 ± 0.02	2.31 ± 0.05	2.26 ± 0.02
rmsd from mean structure			
backbone atoms	0.29[a]	0.62[b]	0.30[c]
heavy atoms	0.70[a]	1.23[b]	0.64[c]
Ramachandran plot			
residues in most favored regions (%)	89.4[a]	90.2[b]	83.4[c]
residues in additionally allowed regions (%)	10.5[a]	8.8[b]	14.7[c]
residues in generously allowed regions (%)	0.2[a]	0.4[b]	0.9[c]
residues in disallowed regions (%)	0[a]	0.6[b]	1.0[c]

[a]Ubiquitin residues 1−73 and Polι UBM2 residues 679−707. [b]Polι UBM2 residues 679−707. [c]Ubiquitin residues 1−73 and Polι UBM2 residues 674−715.

syringe at a concentration of 1.5 mM and wild-type UBM2 in the reaction cell at a concentration of 100 μM. All measurements were paired with control assays to determine the heat of dilution. Data were analyzed by Levenberg−Marquardt nonlinear regression fitting of each ITC isotherm using a model corresponding to one independent binding event.

Protein Data Bank Accession Codes. The atomic coordinates and NMR restraints for human Polι UBM2, Polι UBM2−ubiquitin complex, and Polι UBM2 P692A−ubiquitin complex have been deposited in the Protein Data Bank with accession codes 2L0G, 2KTF, and 2L0F, respectively.

RESULTS AND DISCUSSION

Interaction of Rev1 and Polι UBMs with Ubiquitin. Because of the importance of signaling by ubiquitylation in the regulation of TLS DNA polymerases, we set out to probe the ubiquitin binding mechanism of the conserved ubiquitin-binding motif identified in the Y-family DNA polymerases Rev1 and Polι (Figure 1A) (*28*). Each polymerase has two such motifs (UBM1 and UBM2). We tested several UBM constructs from yeast and human Rev1 and human Polι for expression in *E. coli* and chose to focus on human Polι UBM2 (residues 679−707) because of best quality of NMR spectra.

Incremental addition of nonlabeled Polι UBM2 to ^{15}N-enriched ubiquitin in an NMR spectroscopy titration experiment led to the perturbation of a subset of signals in the ^{1}H−^{15}N HSQC spectrum of ubiquitin and revealed spectral changes characteristic of intermediate to slow exchange between free and UBM2-bound ubiquitin on the NMR chemical shift time scale (Figure 1B).

Residues for which perturbation of resonances were detected in the ^{1}H−^{15}N HSQC spectrum of ubiquitin upon titration with Polι UBM2 belong to the canonical binding site on the β-sheet of ubiquitin that includes Ile44, Val70, and Leu8 (Figure 1C) (*47*). We note, however, that the resonances of Ile44 and Val70 are only moderately affected by the interaction. This is unusual as in the majority of ubiquitin complexes, Ile44, considered the center of interaction, participates in multiple intermolecular contacts (*31*, *48*, *49*).

Complementary NMR titrations of ^{15}N-enriched Polι UBM2 with nonlabeled ubiquitin were also performed (Figure 1D), confirming the interaction and exchange regime. While virtually all UBM2 NMR signals shift upon titration with ubiquitin, the extent of signal dispersion is similar in the absence and presence of ubiquitin (Figure 1D), suggesting that the UBM2 domain does not undergo a folding transition upon binding. As discussed below, there is *cis*−*trans* isomerization of the central Pro692 in free UBM2 while in the complex only the *trans* conformation is present.

The strength of the Polι UBM2−ubiquitin interaction was estimated using ITC (Figure 2). The dissociation constant (K_D) is 23.8 ± 0.9 μM at 10 °C. Analysis of the ITC data also provides a stoichiometry (n) close to unity ($n = 1.01 \pm 0.1$). Under the experimental conditions chosen for ITC measurements (i.e., 50 mM Tris-HCl, pH 7.2, 30 mM NaCl), the binding reaction is endothermic with an observed enthalpy change (ΔH_{obs}) of 4.5 ± 0.4 kcal·mol^{-1} and is entropically favored with $-T\Delta S_{obs} = -10.6 \pm 0.3$ kcal·mol^{-1}.

Structure of Human Polι UBM2−Ubiquitin Complex. To understand the molecular basis of UBM−ubiquitin interaction, we determined the solution structure of the complex of human Polι UBM2 (residues 679−707) and ubiquitin (residues 1−76) using NMR spectroscopy-derived interatomic distance

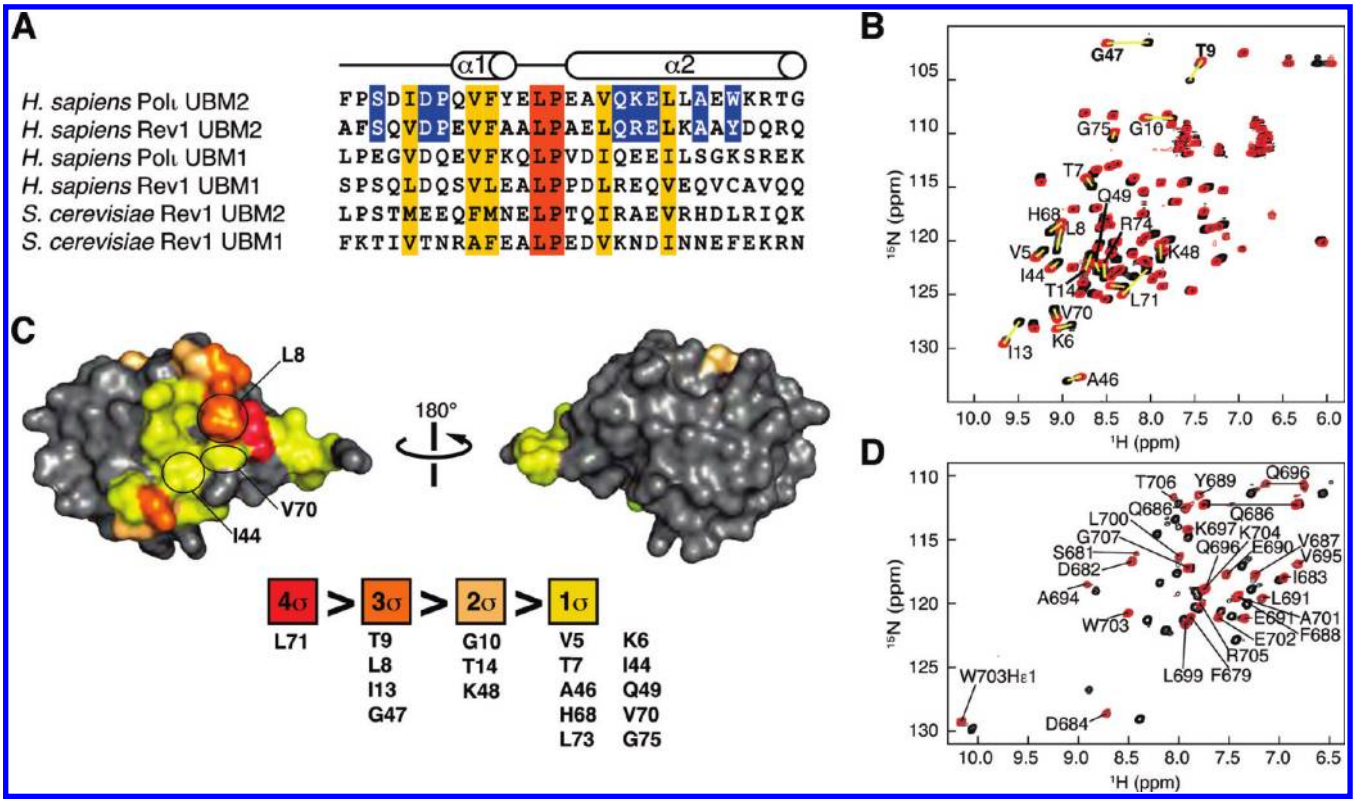

FIGURE 1: Interaction of human Polι UBM2 with ubiquitin. (A) Amino acid sequence alignment of UBMs of human Polι and Rev1 and budding yeast Rev1. Conserved residues in all six UBMs are highlighted in yellow and orange while residues specifically conserved in UBM2 of human Rev1 and Polι are in blue. The secondary structure elements of human Polι UBM2 (i.e., two α-helices) identified from the present study are shown above the alignments. (B) Overlay of nine $^{1}H-^{15}N$ HSQC spectra of ^{15}N-labeled ubiquitin in the free state (black) and after incremental additions of unlabeled Polι UBM2 up to a final ubiquitin:UBM2 molar ratio of 1:3.2 (red). Intermediate spectra are shown in gray. Labeled signals are for residues for which the chemical shift difference between free and bound ubiquitin is at least one standard deviation outside of the mean chemical shift difference. Note that the exchange is intermediate to slow on the time scale of NMR chemical shifts. (C) Surface representation of free ubiquitin with residues exhibiting changes in $^{1}H-^{15}N$ correlation signals color coded for 1, 2, 3, and 4 standard deviations (σ) outside of the mean difference in chemical shifts. (D) $^{1}H-^{15}N$ HSQC spectra of ^{15}N-labeled human Polι UBM2, free (black) and in the presence of a 5-fold molar excess of unlabeled ubiquitin (red). The signals of ubiquitin-bound UBM2 are labeled.

and dihedral angle restraints. The statistics for the structure calculations are summarized in Table 1. As illustrated in Figure 3A, the structure of the complex is well-defined. The average root-mean-square deviation (rmsd) for the 20 lowest energy structures versus the average structure is 0.29 Å when UBM2 (residues 679−707) and ubiquitin (residues 1−73) backbone atoms (N, C^{α}, C′) are included in the calculation and 0.70 Å when all heavy atoms are used.

The structure of UBM2 is comprised of an N-terminal loop region (Phe679−Asp684) and two amphipathic α-helices (α1, Pro685−Tyr689, and α2, Glu693−Gly707) (Figure 3B). The sequence Asp684−Pro685 is a typical α-helix-stabilizing N-cap motif (*50*). This motif is conserved in human Rev1 (Figure 1A). The two α-helices lie at an angle of 52 ± 2° as calculated using interhlx (K. Yap, University of Toronto) and are separated by a conserved leucine (Leu691) and a conserved *trans*-proline residue (Pro692) that precedes the C-terminal α-helix. The overall shape of the complex is that of a disk with contrasting electrostatic properties on each side (Figure 3C). On the binding interface side are the negatively charged residues Asp682, Asp684, Glu690, Glu698, and Glu702 that surround a hydrophobic core, and on the opposite side are the positively charged residues Lys697, Lys704, and Arg705.

The structures of ubiquitin in the free state and in complex with UBM2 are very similar with an rmsd of 1.0 Å for the best-fit superposition of backbone atoms (N, C^{α}, C′) of all residues except the last four of UBM2-bound and free ubiquitin (Protein Data Bank accession code 1UBQ) (*51*).

One hundred thirty-nine unambiguous intermolecular NOEs involving 15 residues of UBM2 and 14 of ubiquitin define the interface between the two proteins (Figure 3F). The total contact surface area is 690 $Å^2$, which is relatively large for a ubiquitin-binding domain (UBD) complex and is consistent with the relatively high affinity of UBM2 (K_D of 23.8 ± 0.9 μM) in comparison to those of other UBDs, with K_D values ranging from 2.8 to 1690 μM (*52*).

The binding interface of ubiquitin and UBM2 is centered on the ubiquitin residue Leu8 (Figure 3D). UBM2 forms a hydrophobic cleft consisting of residues Ile683, Val687, Phe688, Leu691, Leu699, and Trp703 where Leu8 inserts and becomes completely hidden from solvent (Figure 3D). This location of Leu8 is supported by 40 intermolecular NOEs, more than for any other amino acid of the complex. Underscoring the importance of Leu8, mutation of this residue to alanine completely abolishes the interaction of UBM2 with ubiquitin as determined by ITC (Figure 2).

Ubiquitin Ile44 is mostly buried at the intermolecular contact area but is at the edge of the interface and lies on top of a surface formed by UBM2 residues Leu691, Pro692, Val695, and Leu699 (Figure 3D). While central to the majority of UBD−ubiquitin interactions characterized to date, Ile44 contributes in a diminished capacity to the UBM2 recognition, as reflected by a modest

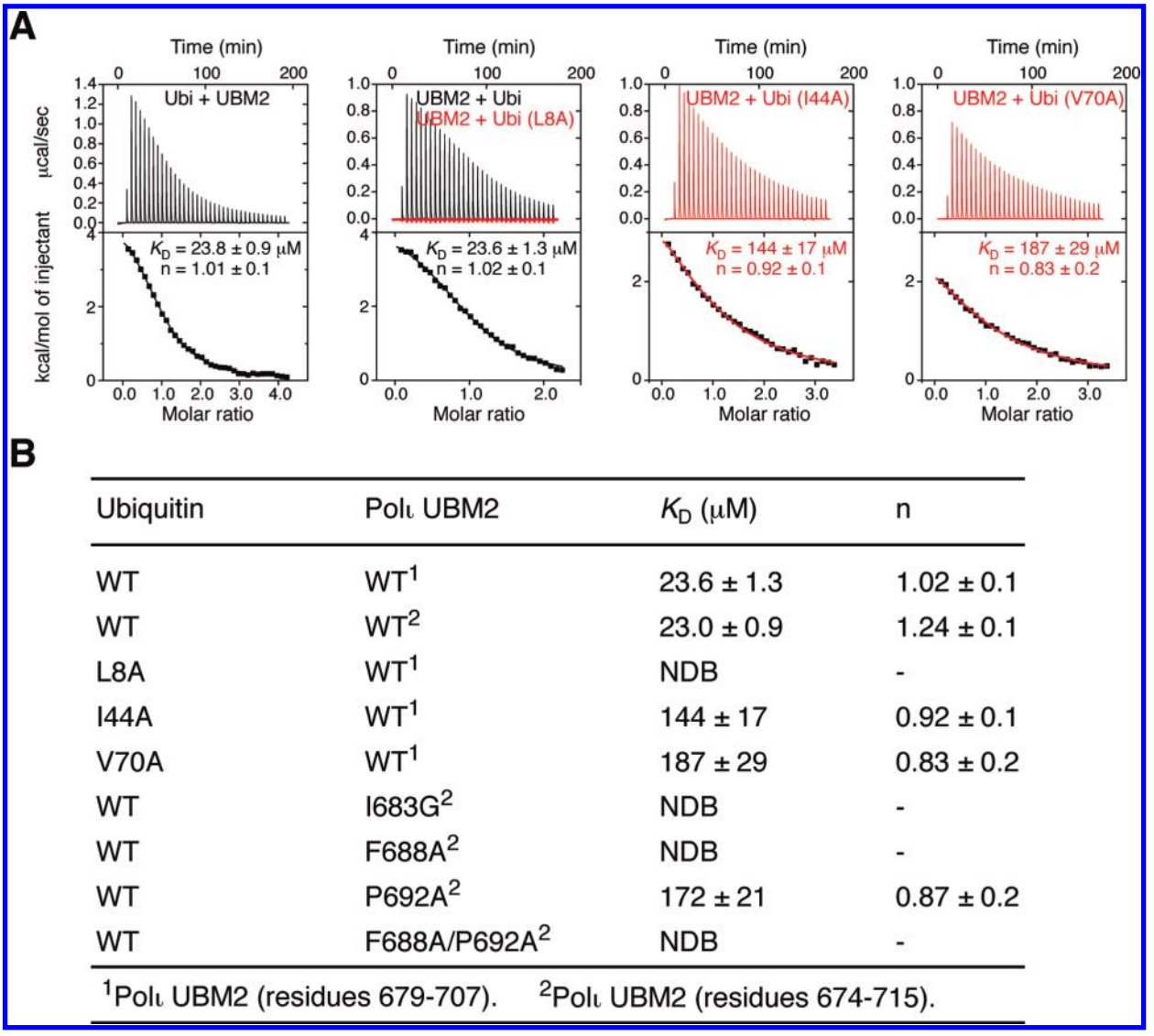

B

Ubiquitin	Polι UBM2	K_D (μM)	n
WT	WT[1]	23.6 ± 1.3	1.02 ± 0.1
WT	WT[2]	23.0 ± 0.9	1.24 ± 0.1
L8A	WT[1]	NDB	-
I44A	WT[1]	144 ± 17	0.92 ± 0.1
V70A	WT[1]	187 ± 29	0.83 ± 0.2
WT	I683G[2]	NDB	-
WT	F688A[2]	NDB	-
WT	P692A[2]	172 ± 21	0.87 ± 0.2
WT	F688A/P692A[2]	NDB	-

[1]Polι UBM2 (residues 679-707). [2]Polι UBM2 (residues 674-715).

FIGURE 2: Polι UBM2−ubiquitin interaction probed by isothermal titration calorimetry. (A) From left to right, representative ITC data for the titrations of wild-type Polι UBM2 with wild-type ubiquitin and of wild-type and mutant ubiquitin (L8A, I44A, and V70A) with wild-type Polι UBM2. All titrations of ubiquitin mutants with UBM2 are highlighted in red. Shown for each experiment are the integrated heat measurements from raw titration data and curve fitting with a standard one-site binding model. K_D and stoichiometry (n) values are indicated with the associated standard deviations determined by nonlinear least-squares fitting. (B) Summary of the effects of point mutations on the interaction of ubiquitin and Polι UBM2 as determined using ITC. K_D and stoichiometry (n) values are indicated with the associated standard deviations determined by nonlinear least-squares fitting. NDB stands for no detectable binding.

6-fold decrease in affinity when mutated to alanine (Figure 2). Consistent with this finding, we note that the UBMs of Y-family polymerases were discovered using a yeast two-hybrid screen with the ubiquitin I44A mutant as bait (*28*).

Ubiquitin Val70 is also buried at the interface and contacts Polι UBM2 residues Leu691, Val695, and Leu699 (Figure 3D). The contribution of Val70 to the strength of interaction with UBM2 is slightly more important than that of Ile44. An approximately 8-fold decrease in the affinity of ubiquitin for UBM2 was measured when Val70 was mutated to alanine (Figure 2).

The four ubiquitin residues Leu8, Ile44, His68, and Val70 define the interacting surface of Polι UBM2. Only the side chain of Leu8, however, is inserted in a deep pocket of UBM2 (Figure 3D). This finding correlates with the ITC data and provides a structural basis for Ile44 playing a secondary role.

In addition to the central hydrophobic core, the interface of ubiquitin and Polι UBM2 also involves charge−charge interactions at its periphery (Figure 3E). The carboxylate groups of Glu698 and Glu702 near the C-terminal end of UBM2 likely form salt bridges with the positively charged ubiquitin residues Arg42, Arg72, and Arg74. A second salt bridge may involve the carboxylate group of UBM2 Glu690 and ubiquitin His68. Finally, the backbone carbonyl group of UBM2 Ser681 and the side chain hydroxyl group of ubiquitin Thr9 are positioned favorably to form a hydrogen bond (Figure 3E).

Another structure of Polι UBM2 bound to ubiquitin was published recently (*53*). Although the UBM2 structure determined in the present study (residues 679−707) has a smaller number of residues compared to that characterized in the other report (residues 676−707; Protein Data Bank accession code 2KHW), the two structures are similar with an overall rmsd of 2.0 Å for the best-fit superposition of backbone atoms (N, C^{α}, C') of UBM2 (residues 679−707) and ubiquitin (residues 1−76).

We note that under the same conditions the K_D of a longer construct of Polι UBM2 (residues 674−715) that we also characterized is comparable to that of Polι UBM2 (residues 679−707),

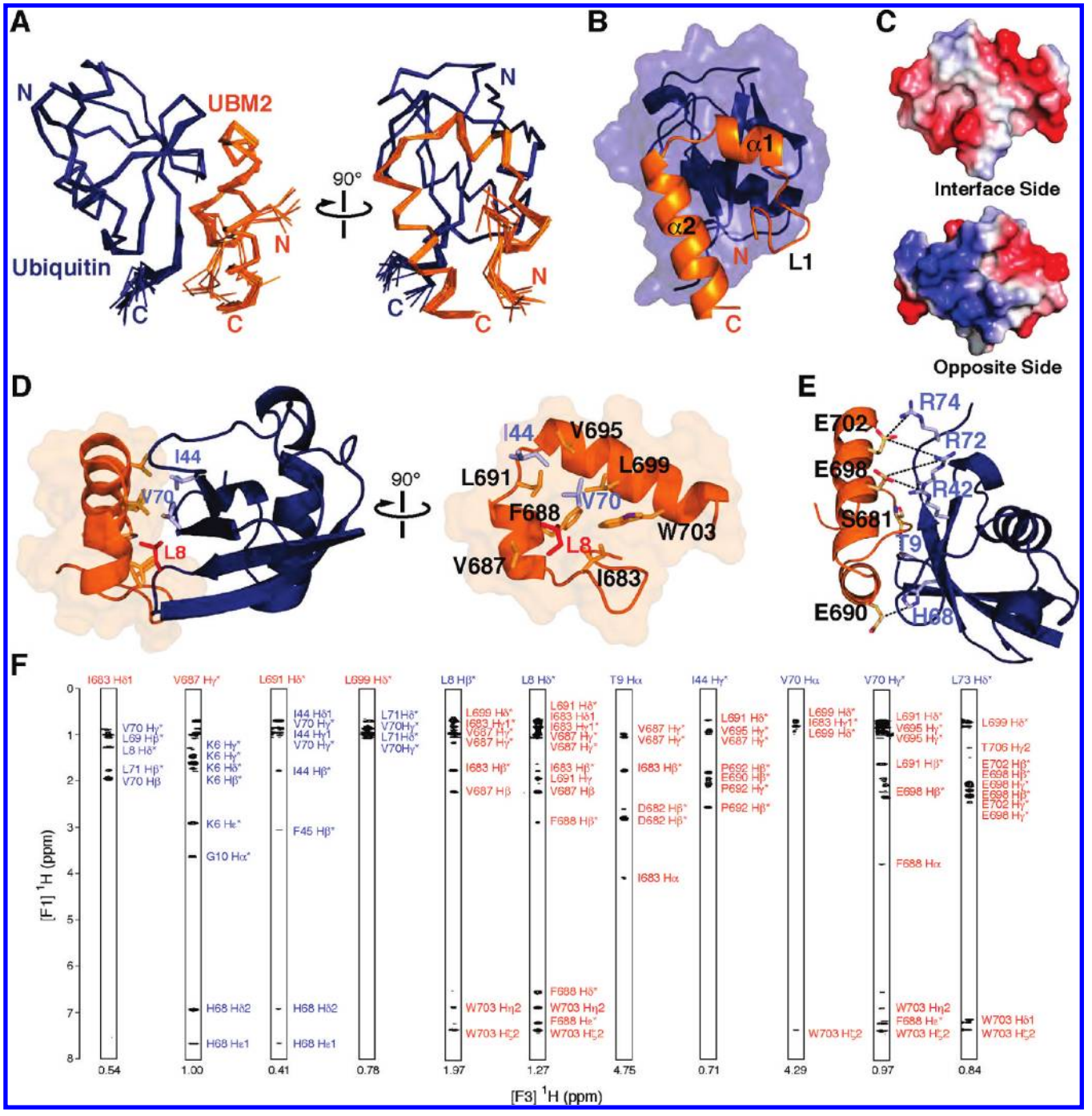

FIGURE 3: Solution structure of Polι UBM2−ubiquitin complex. (A) Superposition of the 20 lowest energy structures of the complex of Polι UBM2 (orange) and ubiquitin (blue) showing the backbone C^{α} atoms. (B) Ribbon representation of the lowest energy structure of Polι UBM2−ubiquitin complex. Polι UBM2 is shown in orange and ubiquitin in blue. (C) Electrostatic surface potential (blue, positive charge; red, negative charge) of Polι UBM2. The ubiquitin interface side and opposite side of Polι UBM2 are shown. (D) Hydrophobic contacts of ubiquitin (blue) and Polι UBM2 (orange). Ubiquitin residues Leu8, Val70, and Ile44 and residues that form the hydrophobic pocket of Polι UBM2 are highlighted. (E) Possible charged interactions and hydrogen bonds between Polι UBM2 and ubiquitin are displayed. (F) Representative intermolecular NOE signals between Polι UBM2 and ubiquitin from the F1 ^{13}C-filtered, F2 ^{13}C-edited NOESY-HSQC spectra. Resonances of UBM2 and ubiquitin are colored orange and blue, respectively.

23.0 ± 0.9 and 23.6 ± 1.3 μM, respectively (Figure 2). The recently published structure of Polι UBM2−ubiquitin was determined with UBM2 fused to the C-terminus of the 56-residue immunoglobulin-binding domain B1 of streptococcal protein G, often used as a solubility enhancement tag (*54*), and includes a $(His)_6$ tag at the C-terminus of UBM2. Our structure is devoid of any tag.

Structure of Free Human Polι UBM2. To probe any possible change in conformation upon complex formation, we determined the structure of Polι UBM2 (residues 679−707) in the absence of ubiquitin (Figure 4A). The average rmsd for the 20 lowest energy structures versus the average structure is 0.62 Å when UBM2 backbone atoms (N, C^{α}, C′) are included in the calculation and 1.23 Å when all heavy atoms are used. The statistics for the structure calculations are summarized in Table 1.

The structure of free Polι UBM2 is similar to its ubiquitin-bound state, with a backbone (N, C^{α}, C′) rmsd of 1.4 Å for the best-fit superposition of residues 679−707. In the free structure,

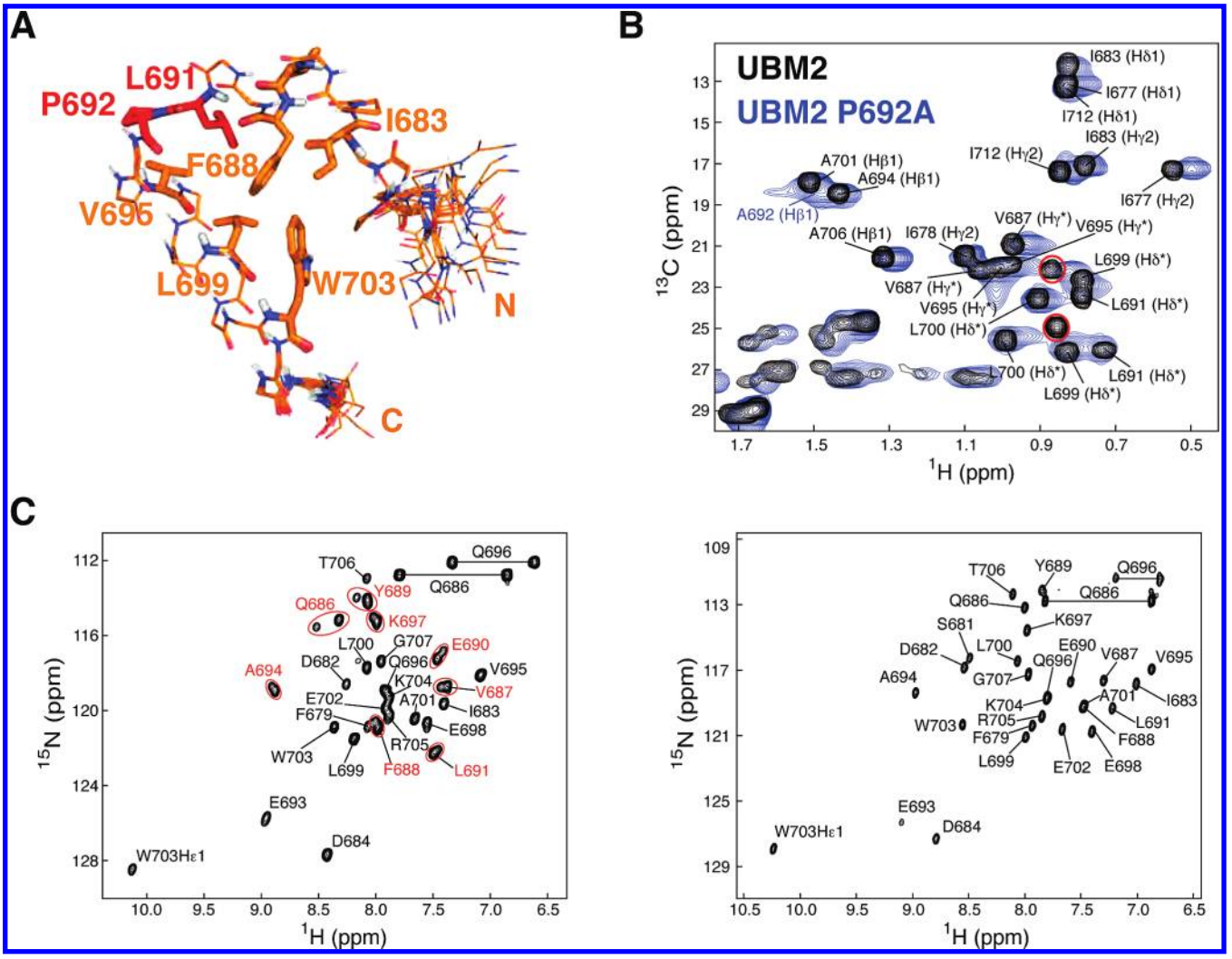

FIGURE 4: Solution structure of Polι UBM2 in the free state. (A) Superposition of the 20 lowest energy structures of Polι UBM2 showing the backbone atoms N, C^{α}, and C′ and selected side chains of the hydrophobic core. Leu691 and Pro692 are highlighted in red. (B) Overlaid methyl region of the $^{1}H-^{13}C$ HSQC spectra of wild-type Polι UBM2 (black) and Polι UBM2 mutant P692A (blue). The additional signals attributed to Leu691 in wild-type UBM2 are circled in red. (C) $^{1}H-^{15}N$ HSQC spectra of wild-type UBM2 in the free state (left) and in complex with ubiquitin (right). Duplicated signals due to Pro692 *cis*−*trans* isomerization are circled in red.

the interhelical angle is 64 ± 3° while it is 52 ± 2° in the ubiquitin-bound form. This small angular difference is within the uncertainty range of NMR spectroscopy-based structure calculations. In conclusion, the UBM2 domain is not stabilized through its interaction with ubiquitin but is independently held together by a hydrophobic core composed of Phe679, Ile683, Phe688, Leu691, Val695, Leu699, and Trp703 (Figure 4A). The side chains previously detailed as shaping the Leu8 binding pocket are still in the same position.

We note that, unlike in the UBM2−ubiquitin complex, in the absence of ubiquitin there is *cis*−*trans* isomerization of the central proline residue of UBM2. This is deduced from comparisons of the $^{1}H-^{13}C$ HSQC spectra of wild-type and P692A mutant UBM2, both in the free state, and $^{1}H-^{15}N$ HSQC spectra of wild-type UBM2 free and bound to ubiquitin. Two sets of methyl signals are attributed to Leu691 in the wild-type protein while there is only one set of Leu691 methyl signals for the P692A mutant protein (Figure 4B). In a similar manner, two sets of amide atom correlation signals are observed for eight residues in free UBM2 while there is only one set of signals in the UMB2−ubiquitin complex (Figure 4C).

There is a second *trans*-proline residue in UBM2 (Pro685) that forms the N-cap of the first α-helix. Pro685, however, is unlikely to populate the *cis* conformation as there is only one set of amide resonances in the $^{1}H-^{15}N$ HSQC spectrum of Polι UBM2 P692A mutant (data not shown). From signal intensities in the $^{1}H-^{13}C$ and $^{1}H-^{15}N$ HSQC spectra, the *cis*-Pro692 population is estimated at ~26%. This relatively small population of *cis*-proline makes it unlikely that *cis*−*trans* isomerization plays a role in the binding process. Nevertheless, the central proline residue is conserved in the UBM1 and UBM2 domains of Polι and Rev1 proteins (Figure 1A) and is important for tight binding (*vide infra*).

Comparison of Polι UBM2−Ubiquitin Complex to Other UBD−Ubiquitin Complexes. Ubiquitin-binding domains, despite their structural heterogeneity, can be categorized into four classes, namely, helical, zinc finger, pleckstrin homology, and ubiquitin-conjugating-like domains (*47*). Notwithstanding their differences, certain conserved ubiquitin binding modes have emerged across these families. In Figure 5, the structure of Polι UBM2−ubiquitin complex is compared to three structures of the helical family of UBDs including MIU (motif interacting with ubiquitin) of Rabex5 (*55*), UBA (ubiquitin associated) of Dsk2 (*56*), and DUIM (double-sided ubiquitin interacting motif) of HRS (*57*).

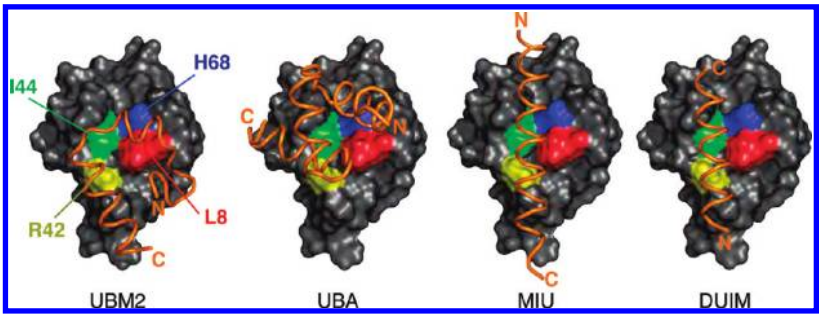

FIGURE 5: Comparison of Polι UBM2 to other helical ubiquitin-binding domains. Ubiquitin (surface representation, gray) in complex with four different ubiquitin-binding domains (ribbon representation, orange), namely, Polι UBM2, this study; Dsk2-UBA, PDB 1WR1; Rabex5-MIU, PDB 2FIF; and HRS-DUIM, PDB 2D3G. Ubiquitin orientation is fixed with its Leu8, Arg42, Ile44, and His68 residues highlighted. UBM2 interacts primarily with ubiquitin Leu8 while UBA, MIU, and DUIM center on ubiquitin Ile44 for binding.

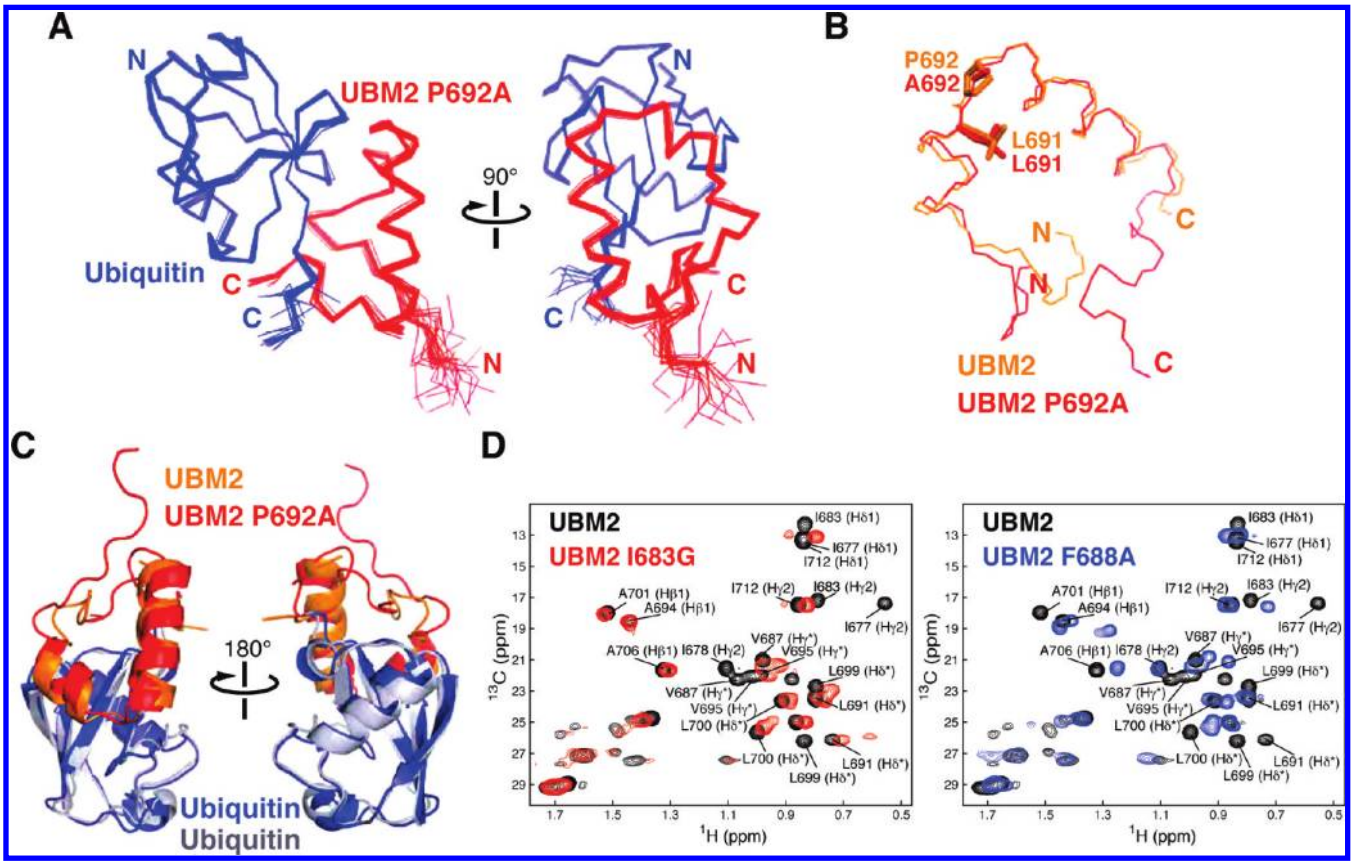

FIGURE 6: Structure of Polι UBM2 P692A bound to ubiquitin and comparison to the structure of wild-type Polι UBM2−ubiquitin complex. (A) Superposition of the 20 lowest energy structures of the complex of Polι UBM2 P692A mutant (red) and ubiquitin (blue) showing the backbone C^{α} atoms. (B) Overlay of the backbone atoms N, C^{α}, and C′ of wild-type Polι UBM2 (orange) and P692A mutant (red), both from the structures of their complex with ubiquitin. Shown are residues Leu691 and Pro692 in wild-type UBM2 (orange) and Leu691 and Ala692 in UBM2 P692A mutant (red). (C) Structures of Polι UBM2 wild-type (orange) and P692A mutant (red), both in complex with ubiquitin (blue and gray, respectively). (D) Overlaid methyl region of the ^{1}H−^{13}C HSQC spectra of wild-type Polι UBM2 (black) and Polι UBM2 mutants I683G (red) and F688A (blue).

A central feature of the vast majority of ubiquitin−UBD interactions is the involvement of the hydrophobic residues Leu8, Ile44, and Val70 of ubiquitin. All of the domains shown in Figure 5 but Polι UBM2 are centered on ubiquitin Ile44 where a hydrophobic patch on the UBD makes favorable contacts with this residue. Illustrative of its importance, mutation of Ile44 abolishes or greatly weakens the affinity for the corresponding UBDs (*47*, *52*, *58*). The structure of the Polι UBM2−ubiquitin complex shows that ubiquitin Ile44 lies away from the central hydrophobic patch of Polι. Consistent with this observation, we find that the I44A mutation in ubiquitin only has a limited effect on the interaction with Polι UBM2 (Figure 2).

Determinants of the UBM Fold. The structure of Polι UBM2 has similarities to the helical MIU and DUIM structures mentioned above (Figure 5), notably the conservation of negatively charged residues at the C-terminal end of the second α-helix that are in the vicinity of several arginines (Arg42, Arg72, Arg74) of ubiquitin. A major difference, however, is the conserved central proline residue (Pro692) in Polι UBM2 that separates its two α-helices. Presumably, this is also the case in Polι UBM1 and Rev1 UBM1 and UBM2.

To address the possibility that Pro692 might contribute to the sharp bent between the two α-helices of UBM2, contrasting with the long straight α-helix in MIU and DUIM (Figure 5), we

determined the solution structure of the complex of human Polι UBM2 P692A (residues 674−715) and ubiquitin using NMR spectroscopy (Figure 6A). The average rmsd for the 20 lowest energy structures versus the average structure is 0.30 Å when UBM2 P692A (residues 674−715) and ubiquitin (residues 1−73) backbone atoms (N, C^{α}, C′) are used in the calculation and 0.64 Å when all heavy atoms are included. The statistics for the structure calculations are summarized in Table 1. While affinity is reduced by approximately 7-fold compared to that of wild-type Polι UBM2 (K_D = 172 ± 21 μM) (Figure 2B), in the complex with ubiquitin the structure of Polι UBM2 P692A is relatively unchanged from the wild-type structure with an rmsd of 1.1 Å when the backbone atoms (N, C^{α}, C′) of residues 684−707 are included in the calculation (Figure 6B). The interhelical angle of 55 ± 1° is comparable to that of wild-type UBM2 (52 ± 2°). Pro692 is therefore not required for the sharp interhelical kink to occur.

An overlay of Polι UBM2−ubiquitin and Polι UBM2 P692A−ubiquitin structures shows that the two complexes are similar (Figure 6C). Any small difference between the two structures likely reflects the uncertainty in structure calculations. Therefore, the ~7-fold decrease in affinity of the P692A mutant is probably due to the reduced contribution of Ala692 to van der Waals contacts compared to Pro692.

Interestingly, Ile712, not present in our structure of wild-type Polι UBM2−ubiquitin nor in the previously published structure, has 12 intermolecular NOEs with ubiquitin Leu69, Val70, Leu71, and Leu73 and 40 intramolecular NOEs with 17 other UBM2 residues, which extends the hydrophobic core of UBM2 and closes its triangle-like structure contacting the Ile44-, Val70-, and Leu8-containing surface of ubiquitin. It is clear from the similarity of the $^{1}H-^{13}C$ HSQC spectra that this extended hydrophobic core is also present in the longer version of wild-type Polι UBM2 (residues 674−715) (data not shown).

To probe the contribution of Polι UBM2 hydrophobic contacts in defining the UBM fold and ubiquitin recognition mechanism, we mutated Ile683 and Phe688, two residues of the hydrophobic core. Replacement of Ile683 by a glycine and Phe688 by an alanine or a serine led to total loss of interaction (Figure 2B). There are major changes in the $^{1}H-^{13}C$ HSQC spectra of the I683G and F688A UBM2 mutants compared to the wild-type protein spectrum, in particular a decrease in signal dispersion in the methyl group region of the spectra (Figure 6D). This is a clear indication that the UBM2 fold is disrupted by the mutations. These observations indicate that the UBM fold and ubiquitin binding mode are defined by the hydrophobic core.

CONCLUSION

The UBM domains of polymerase ι and Rev1 are important for the regulation of translesion DNA synthesis through their interaction with monoubiquitylated PCNA. Presented here are the structures of Polι UBM2, free and in complex with ubiquitin, revealing a new mechanism for ubiquitin recognition, as also recently reported by others (*53*). While there are some similarities between Polι UBM2 and other ubiquitin-binding domains, the unique characteristic of the Polι UBM2−ubiquitin structure is the centrality of ubiquitin Leu8 instead of Ile44 as the primary intermolecular contact. This ubiquitin recognition mechanism is defined by the kinked two-helix fold of UBM2 that surrounds Leu8. While a conserved proline residue separates the two α-helices in the UBM domain, we showed that the sharp angle between the two helices is proline-independent and is determined by long-range hydrophobic packing interactions.

ACKNOWLEDGMENT

We thank Patricia Kannouche (Université Paris-Sud, France), F. Peter Guengerich (Vanderbilt University, TN), and Robert Piper (University of Iowa, IA) for reagents. We thank Marina Ramirez-Alvarado and Laura Sikkink (Mayo Clinic, MN) for advice and assistance with circular dichroism measurements. We are grateful to Namit Singh (Mayo Clinic, MN) for careful reading of the manuscript and helpful suggestions.

REFERENCES

1. Friedberg, E. C. (2005) Suffering in silence: the tolerance of DNA damage. *Nat. Rev. Mol. Cell Biol. 6*, 943–953.
2. Yang, W., and Woodgate, R. (2007) What a difference a decade makes: insights into translesion DNA synthesis. *Proc. Natl. Acad. Sci. U.S.A. 104*, 15591–15598.
3. Guo, C., Kosarek-Stancel, J. N., Tang, T. S., and Friedberg, E. C. (2009) Y-family DNA polymerases in mammalian cells. *Cell. Mol. Life Sci. 66*, 2363–2381.
4. Ohmori, H., Friedberg, E. C., Fuchs, R. P., Goodman, M. F., Hanaoka, F., Hinkle, D., Kunkel, T. A., Lawrence, C. W., Livneh, Z., Nohmi, T., Prakash, L., Prakash, S., Todo, T., Walker, G. C., Wang, Z., and Woodgate, R. (2001) The Y-family of DNA polymerases. *Mol. Cell 8*, 7–8.
5. Ling, H., Boudsocq, F., Woodgate, R., and Yang, W. (2001) Crystal structure of a Y-family DNA polymerase in action: a mechanism for error-prone and lesion-bypass replication. *Cell 107*, 91–102.
6. Zhou, B. L., Pata, J. D., and Steitz, T. A. (2001) Crystal structure of a DinB lesion bypass DNA polymerase catalytic fragment reveals a classic polymerase catalytic domain. *Mol. Cell 8*, 427–437.
7. Trincao, J., Johnson, R. E., Escalante, C. R., Prakash, S., Prakash, L., and Aggarwal, A. K. (2001) Structure of the catalytic core of *S. cerevisiae* DNA polymerase eta: implications for translesion DNA synthesis. *Mol. Cell 8*, 417–426.
8. Hoege, C., Pfander, B., Moldovan, G. L., Pyrowolakis, G., and Jentsch, S. (2002) RAD6-dependent DNA repair is linked to modification of PCNA by ubiquitin and SUMO. *Nature 419*, 135–141.
9. Lemontt, J. F. (1971) Mutants of yeast defective in mutation induced by ultraviolet light. *Genetics 68*, 21–33.
10. Jansen, J. G., Tsaalbi-Shtylik, A., Langerak, P., Calleja, F., Meijers, C. M., Jacobs, H., and de Wind, N. (2005) The BRCT domain of mammalian Rev1 is involved in regulating DNA translesion synthesis. *Nucleic Acids Res. 33*, 356–365.
11. Guo, C., Sonoda, E., Tang, T. S., Parker, J. L., Bielen, A. B., Takeda, S., Ulrich, H. D., and Friedberg, E. C. (2006) REV1 protein interacts with PCNA: significance of the REV1 BRCT domain *in vitro* and *in vivo*. *Mol. Cell 23*, 265–271.
12. Garg, P., and Burgers, P. M. (2005) Ubiquitinated proliferating cell nuclear antigen activates translesion DNA polymerases eta and REV1. *Proc. Natl. Acad. Sci. U.S.A. 102*, 18361–18366.
13. Haracska, L., Unk, I., Prakash, L., and Prakash, S. (2006) Ubiquitylation of yeast proliferating cell nuclear antigen and its implications for translesion DNA synthesis. *Proc. Natl. Acad. Sci. U.S.A. 103*, 6477–6482.
14. Friedberg, E. C. (2006) Reversible monoubiquitination of PCNA: a novel slant on regulating translesion DNA synthesis. *Mol. Cell 22*, 150–152.
15. Nelson, J. R., Lawrence, C. W., and Hinkle, D. C. (1996) Deoxycytidyl transferase activity of yeast REV1 protein. *Nature 382*, 729–731.
16. Prakash, S., Johnson, R. E., and Prakash, L. (2005) Eukaryotic translesion synthesis DNA polymerases: specificity of structure and function. *Annu. Rev. Biochem. 74*, 317–353.
17. Friedberg, E. C., Lehmann, A. R., and Fuchs, R. P. (2005) Trading places: how do DNA polymerases switch during translesion DNA synthesis? *Mol. Cell 18*, 499–505.
18. Waters, L. S., Minesinger, B. K., Wiltrout, M. E., D'Souza, S., Woodruff, R. V., and Walker, G. C. (2009) Eukaryotic translesion polymerases and their roles and regulation in DNA damage tolerance. *Microbiol. Mol. Biol. Rev. 73*, 134–154.
19. Guo, C., Fischhaber, P. L., Luk-Paszyc, M. J., Masuda, Y., Zhou, J., Kamiya, K., Kisker, C., and Friedberg, E. C. (2003) Mouse Rev1 protein interacts with multiple DNA polymerases involved in translesion DNA synthesis. *EMBO J. 22*, 6621–6630.

20. D'Souza, S., and Walker, G. C. (2006) Novel role for the C terminus of *Saccharomyces cerevisiae* Rev1 in mediating protein-protein interactions. *Mol. Cell. Biol. 26*, 8173–8182.
21. Acharya, N., Haracska, L., Prakash, S., and Prakash, L. (2007) Complex formation of yeast Rev1 with DNA polymerase eta. *Mol. Cell. Biol. 27*, 8401–8408.
22. Kosarek, J. N., Woodruff, R. V., Rivera-Begeman, A., Guo, C., D'Souza, S., Koonin, E. V., Walker, G. C., and Friedberg, E. C. (2008) Comparative analysis of *in vivo* interactions between Rev1 protein and other Y-family DNA polymerases in animals and yeasts. *DNA Repair* (*Amsterdam*) *7*, 439–451.
23. Haracska, L., Johnson, R. E., Unk, I., Phillips, B., Hurwitz, J., Prakash, L., and Prakash, S. (2001) Physical and functional interactions of human DNA polymerase eta with PCNA. *Mol. Cell. Biol. 21*, 7199–7206.
24. Vidal, A. E., Kannouche, P., Podust, V. N., Yang, W., Lehmann, A. R., and Woodgate, R. (2004) Proliferating cell nuclear antigen-dependent coordination of the biological functions of human DNA polymerase iota. *J. Biol. Chem. 279*, 48360–48368.
25. Haracska, L., Acharya, N., Unk, I., Johnson, R. E., Hurwitz, J., Prakash, L., and Prakash, S. (2005) A single domain in human DNA polymerase iota mediates interaction with PCNA: implications for translesion DNA synthesis. *Mol. Cell. Biol. 25*, 1183–1190.
26. Acharya, N., Yoon, J. H., Gali, H., Unk, I., Haracska, L., Johnson, R. E., Hurwitz, J., Prakash, L., and Prakash, S. (2008) Roles of PCNA-binding and ubiquitin-binding domains in human DNA polymerase eta in translesion DNA synthesis. *Proc. Natl. Acad. Sci. U.S.A. 105*, 17724–17729.
27. Hishiki, A., Hashimoto, H., Hanafusa, T., Kamei, K., Ohashi, E., Shimizu, T., Ohmori, H., and Sato, M. (2009) Structural basis for novel interactions between human translesion synthesis polymerases and proliferating cell nuclear antigen. *J. Biol. Chem. 284*, 10552–10560.
28. Bienko, M., Green, C. M., Crosetto, N., Rudolf, F., Zapart, G., Coull, B., Kannouche, P., Wider, G., Peter, M., Lehmann, A. R., Hofmann, K., and Dikic, I. (2005) Ubiquitin-binding domains in Y-family polymerases regulate translesion synthesis. *Science 310*, 1821–1824.
29. Wood, A., Garg, P., and Burgers, P. M. (2007) A ubiquitin-binding motif in the translesion DNA polymerase Rev1 mediates its essential functional interaction with ubiquitinated proliferating cell nuclear antigen in response to DNA damage. *J. Biol. Chem. 282*, 20256–20263.
30. Guo, C., Tang, T. S., Bienko, M., Parker, J. L., Bielen, A. B., Sonoda, E., Takeda, S., Ulrich, H. D., Dikic, I., and Friedberg, E. C. (2006) Ubiquitin-binding motifs in REV1 protein are required for its role in the tolerance of DNA damage. *Mol. Cell. Biol. 26*, 8892–8900.
31. Bomar, M. G., Pai, M. T., Tzeng, S. R., Li, S. S., and Zhou, P. (2007) Structure of the ubiquitin-binding zinc finger domain of human DNA Y-polymerase eta. *EMBO Rep. 8*, 247–251.
32. Botuyan, M. V., Nominé, Y., Yu, X., Juranic, N., Macura, S., Chen, J., and Mer, G. (2004) Structural basis of BACH1 phosphopeptide recognition by BRCA1 tandem BRCT domains. *Structure 12*, 1137–1146.
33. Piotrowski, J., Beal, R., Hoffman, L., Wilkinson, K. D., Cohen, R. E., and Pickart, C. M. (1997) Inhibition of the 26 S proteasome by polyubiquitin chains synthesized to have defined lengths. *J. Biol. Chem. 272*, 23712–23721.
34. Sundd, M., Iverson, N., Ibarra-Molero, B., Sanchez-Ruiz, J. M., and Robertson, A. D. (2002) Electrostatic interactions in ubiquitin: stabilization of carboxylates by lysine amino groups. *Biochemistry 41*, 7586–7596.
35. Bax, A., Clore, G. M., and Gronenborn, A. M. (1990) ^{1}H-^{1}H correlation via isotropic mixing of ^{13}C magnetization, a new three-dimensional approach for assigning ^{1}H and ^{13}C spectra of ^{13}C-enriched proteins. *J. Magn. Reson. 88*, 425–431.
36. Ferentz, A. E., and Wagner, G. (2000) NMR spectroscopy: a multifaceted approach to macromolecular structure. *Q. Rev. Biophys. 33*, 29–65.
37. Zwahlen, C., Legault, P., Vincent, S. J. F., Greenblat, J., Konrat, R., and Kay, L. E. (1997) Methods of measurements of intermolecular NOEs by multinuclear NMR spectroscopy: application to a bacteriophage N-peptide/box B RNA complex. *J. Am. Chem. Soc. 119*, 6711–6721.
38. Delaglio, F., Grzesiek, S., Vuister, G. W., Zhu, G., Pfeifer, J., and Bax, A. (1995) NMRPipe: a multidimensional spectral processing system based on UNIX pipes. *J. Biomol. NMR 6*, 277–293.
39. Johnson, B. A., and Blevins, R. A. (1994) NMRView: a computer program for visualization and analysis of NMR data. *J. Biomol. NMR 4*, 603–614.
40. Cornilescu, G., Delaglio, F., and Bax, A. (1999) Protein backbone angle restraints from searching a database for chemical shift and sequence homology. *J. Biomol. NMR 13*, 289–302.
41. Wishart, D. S., and Sykes, B. D. (1994) The ^{13}C chemical-shift index: a simple method for the identification of protein secondary structure using ^{13}C chemical-shift data. *J. Biomol. NMR 4*, 171–180.
42. Güntert, P. (2004) Automated NMR structure calculation with CYANA. *Methods Mol. Biol. 278*, 353–378.
43. Duggan, B. M., Legge, G. B., Dyson, H. J., and Wright, P. E. (2001) SANE (Structure Assisted NOE Evaluation): an automated model-based approach for NOE assignment. *J. Biomol. NMR 19*, 321–329.
44. Case, D. A., Cheatham, T. E., III, Darden, T., Gohlke, H., Luo, R., Merz, K. M., Jr., Onufriev, A., Simmerling, C., Wang, B., and Woods, R. J. (2005) The Amber biomolecular simulation programs. *J. Comput. Chem. 26*, 1668–1688.
45. Bashford, D., and Case, D. A. (2000) Generalized born models of macromolecular solvation effects. *Annu. Rev. Phys. Chem. 51*, 129–152.
46. Laskowski, R. A., Rullmannn, J. A., MacArthur, M. W., Kaptein, R., and Thornton, J. M. (1996) AQUA and PROCHECK-NMR: programs for checking the quality of protein structures solved by NMR. *J. Biomol. NMR 8*, 477–486.
47. Dikic, I., Wakatsuki, S., and Walters, K. J. (2009) Ubiquitin-binding domains—from structures to functions. *Nat. Rev. Mol. Cell Biol. 10*, 659–671.
48. Swanson, K. A., Kang, R. S., Stamenova, S. D., Hicke, L., and Radhakrishnan, I. (2003) Solution structure of Vps27 UIM-ubiquitin complex important for endosomal sorting and receptor downregulation. *EMBO J. 22*, 4597–4606.
49. Schreiner, P., Chen, X., Husnjak, K., Randles, L., Zhang, N., Elsasser, S., Finley, D., Dikic, I., Walters, K. J., and Groll, M. (2008) Ubiquitin docking at the proteasome through a novel pleckstrin-homology domain interaction. *Nature 453*, 548–552.
50. Richardson, J. S., and Richardson, D. C. (1988) Amino acid preferences for specific locations at the ends of α-helices. *Science 240*, 1648–1652.
51. Vijay-Kumar, S., Bugg, C. E., and Cook, W. J. (1987) Structure of ubiquitin refined at 1.8 Å resolution. *J. Mol. Biol. 194*, 531–544.
52. Hurley, J. H., Lee, S., and Prag, G. (2006) Ubiquitin-binding domains. *Biochem. J. 399*, 361–372.
53. Bomar, M. G., D'Souza, S., Bienko, M., Dikic, I., Walker, G. C., and Zhou, P. (2010) Unconventional ubiquitin recognition by the ubiquitin-binding motif within the Y family DNA polymerases iota and Rev1. *Mol. Cell 37*, 408–417.
54. Zhou, P., and Wagner, G. (2010) Overcoming the solubility limit with solubility-enhancement tags: successful applications in biomolecular NMR studies. *J. Biomol. NMR 46*, 23–31.
55. Lee, S., Tsai, Y. C., Mattera, R., Smith, W. J., Kostelansky, M. S., Weissman, A. M., Bonifacino, J. S., and Hurley, J. H. (2006) Structural basis for ubiquitin recognition and autoubiquitination by Rabex-5. *Nat. Struct. Mol. Biol. 13*, 264–271.
56. Ohno, A., Jee, J., Fujiwara, K., Tenno, T., Goda, N., Tochio, H., Kobayashi, H., Hiroaki, H., and Shirakawa, M. (2005) Structure of the UBA domain of Dsk2p in complex with ubiquitin molecular determinants for ubiquitin recognition. *Structure 13*, 521–532.
57. Hirano, S., Kawasaki, M., Ura, H., Kato, R., Raiborg, C., Stenmark, H., and Wakatsuki, S. (2006) Double-sided ubiquitin binding of Hrs-UIM in endosomal protein sorting. *Nat. Struct. Mol. Biol. 13*, 272–277.
58. Hofmann, K. (2009) Ubiquitin-binding domains and their role in the DNA damage response. *DNA Repair* (*Amsterdam*) *8*, 544–556.